UDC 621.35 doi: 10.33609/0041-6045.85.12.2019.96-109

**T.A.Nenastina[2], M.V.Ved'[1]*, N.D.Sakhnenko[1], I.Yu.Yermolenko[1], V.A.Proskurina[1], M.M.Volobuyev[1]**

# CORROSION BEHAVIOR OF THE ELECTROLYTIC TERNARY COBALT ALLOYS WITH Mo(W) AND Zr IN ALKALINE SOLUTION

*[1]National Technical University "Kharkiv Polytechnic Institute", 2 Kyrpychova Str., Kharkiv, 61002, Ukraine [2]Kharkiv National Automobile and Highway University,25 Yaroslava Mudrogo Str., Kharkiv , Ukraine*
**e-mail: vmv@kpi.kharkov.ua*

The ternary Co–Mo–W(Zr) coatings with total content of refractory metals of 30–40 wt.%, and Co–W–Zr alloys (12–26 wt.%) are deposited from pyrophosphate-citrate electrolytes in pulse regime. The composition of the coatings as well as the surface morphology depends on the current density. The X-ray diffraction patterns reflect the amorphous-and-crystalline ternary alloys structure. Phases of α-Co, Co–Mo intermetallic compounds, and traces of metallic molybdenum were detected in the Co–Mo–Zr coatings. Phase composition of Co–Mo–W deposits differs by emergence of Co7W6 phase and traces of metallic tungsten, and there is no metallic W in Co–W–Zr electrolytic alloys. The corrosion behavior of ternary coatings in alkaline medium studied by EIS shows that Co–Mo–Zr alloys are characterized by highest corrosion resistance among deposited coatings due to presence of metallic molybdenum and stoichiometric $ZrO_2$ with both high electrical resistivity and chemical stability. The coatings Co–Mo–W and Co–Mo–Zr containing phases of Mo or W are characterized by higher corrosion resistance as compared with that without metallic molybdenum and tungsten. The cyclic voltammetry data confirm stability of ternary coatings in alkaline solution under anodic polarization. Such properties as well as the developed globular surface make materials promising for use as anodes in fuel cells in particular based on alkali electrolytes.

K e y w o r d s: electrodeposition, cobalt alloys, corrosion resistance, refractory metal.

*INTRODUCTION*. The development of efficient power supply sources (PSS) has always been and remains to be one of the most promising areas that ensure energy stability of any country. A wide range of PPSs also includes fuel cells (FC) as the most ecologically safe and promising energy sources, because the reactions in them are reduced to the formation of water from the fuel, in particular, hydrogen and oxygen [1–

3]. A sticking point of FC is electrode materials, which act as catalytic agents. In the vast majority of cases these are expensive materials related to the platinum and silver family [4–6]. In addition to their high electrocatalytic activity such materials differ by their stability and chemical resistance when exposed to the media of different mineralization and corrosiveness. Earlier researches [7–11] show that alloys based on transition metals can be regarded as decent competitors to precious metals.

The main requirements to the catalysts can be expressed as three properties: high catalytic activity, chemical and corrosion resistance, and nontoxicity [12, 13]. Undoubtedly, the activity of catalysts is defined by the material nature though it depends to a great extent on the surface condition. It is known that molybdenum compounds possess certain catalytic activity regarding many processes, for example, electrochemical methanol oxidation, reduction of iodates, oxygen, etc. [14]. Cobalt compounds, such as oxides and complexes, are also applied in electrocatalysis [15]. Evidently, it is related to the mobility of oxygen contained by the compounds of metals, their high coordination capacity, and ability to form nonstoichiometric oxides [16].

The use of alkaline electrolytes allows extending the range of materials that can be used for the formation of catalytic matrixes. It is conditioned by the acceleration of the reduction reaction of oxygen, and simple alcohols in alkaline electrolytes in comparison with acid electrolytes [17], and a lower corrosiveness of the former with regard to many transition metals.

Hence, the formation of the layer of electrolytic alloys based on cobalt with molybdenum (tungsten) and zirconium that has a branched globular surface can provide a preset route for the methanol electro-oxidation process and increase the FC operation efficiency without using precious metals. It should be noted that the scientific and technical literature contains information on the corrosion resistance of cobalt alloys mainly in chloride-containing neutral media [11, 18–21]. So, the subject of this paper is the investigation of corrosion stability of cobalt alloys, including the studies of the corrosion resistance and anodic behavior of ternary cobalt alloys with refractory metals in alkaline medium.

*EXPERIMENT AND DISCUSSION OF THE RESULTS*. The corrosion resistance was investigated using electrodes with electrolytic coatings of ternary Co–Mo–W, Co–Mo–Zr, and Co–W–Zr alloys of thickness at least 5 μm. The coatings were applied onto the steel substrate from the biligand pyrophosphate-citrate electrolytes [9, 22]. The samples were subjected to the preliminary treatment using the methods given in [23]. The electrodeposition was conducted using the pulse current at a varied current density, pulse frequency, and on/off time ratio [9, 22]. The electrolyte temperature was maintained at 30–35 °C.

Chemical composition of the coatings was determined by energy dispersive X-ray spectroscopy by an Oxford INCA Energy 350 electron probe microanalysis integrated into the system of the SEM. The X-rays were excited by exposure of the samples to a beam of 15 keV electrons. The surface morphology of the deposits was studied with

a Zeiss EVO 40XVP scanning electron microscope (SEM). Images were made registering secondary electrons (SEs) via scanning with an electron beam; this mode made possible to study the topography with a high resolution and contrast ratio.

The surface relief and morphology were evaluated by the contact method on 10×10×2 mm samples with an NT-206 scanning probe AFM microscope (lateral and vertical resolutions 2 and 0.2 nm, respectively; 1024×1024 scanning matrix, CSC cantilever B as a probe, probe tip radius being 10 nm) [24–26].

The structure of the coatings deposited onto the copper substrate was examined by X-ray diffraction analysis using a diffractometer (DRON-3.0) in the emission of cobalt anode and CuKα radiation. The compounds (phases) were identified by the method of comparison of interplane distances ($d$, A), and relative intensities ($I/I^0$) of the experimental curve with electron PCPDFWIN card index data.

The polarization dependences for Co–Mo–W(Zr) electrodes in 0.25M NaOH were obtained using the potentiostat PI-50.1.1, and the programmer PR-8 equipped with the special device intended for the digital data registration. Cyclic voltammetry data (CV) were analyzed at the potential scanning rate of $s$ = 0.002–0.05 V/s according to the algorithm given in [27]. A standard three-electrode cell was used for the measurements, a platinum spiral served as an auxiliary electrode, and a reference electrode was saturated silver-chloride connected to the cell via a salt bridge. All electrode potentials in the paper are given vs Standard Hydrogen Electrode (SHE).

The coating corrosion resistance was studied using the method of electrode impedance in the model solution of 0.25M NaOH. The electrochemical impedance spectra (EIS) of the electrodes with the coatings that have a working area of 1cm$^2$ arranged at a distance of 1 cm from each other in the two-electrode cell were registered in the frequency range of $10^{-2}$–$10^6$ Hz at the free corrosion potential using the electrochemical module Autolab-30 (type PGSTAT301N Metrohm Autolab) equipped with the frequency response analyzer module (type FRA-2). The measurements were performed at 18–1 °C. The module was controlled using the Autolab 4.9 program according to the standard procedure with the subsequent processing by the Zview 2.0 package. The phase interface structure was simulated using the method of equivalent circuits. The EIS results are discussed according to known approaches [28, 29].

The coatings formed by ternary Co–Mo–W alloys (table 1, specimens 1, 2) are characterized by the uniformly branched globular surface whose relief differs considerably from that of the substrate onto which these are applied (fig. 1, *a*, *b*). We can see the cracks and a number of pores on the surface of specimen 2 (fig. 2) which is coated with Co–Mo–W at the current density 6 A/dm$^2$. This phenomenon can be explained by two reasons. First, a higher rate of nucleation and growth of crystallites at a higher current density leads to an increase in internal stresses in coatings and following cracking. Second, the hydrogen evolution reaction is intensified with increasing polarization, and causes the porosity of

T a b l e 1

**Effect of the current density *i* and pulse/pause duration ($t_{on}/t_{off}$) on the composition of the ternary cobalt coatings**

| Specimen | Electrolysis regime | | Composition, wt.% (in the terms of metal) |
|---|---|---|---|
| | $i$, A/dm$^2$ | $t_{on}/t_{off}$, ms | |
| 1 (Co–Mo–W) | 4 | 2/10 | Co –59.94; Mo –23.28; W – 16.77 |
| 2 (Co–Mo–W) | 6 | 2/10 | Co – 61.06; Mo – 20.58; W – 18.36 |
| 3 (Co–Mo–Zr) | 4 | 2/10 | Co – 62.13; Mo – 33.29; Zr – 4.58 |
| 4 (Co–Mo–Zr) | 4 | 5/10 | Co – 63.61; Mo – 32.60; Zr – 3.79 |
| 5 (Co–Mo–Zr) | 6 | 5/10 | Co – 68.96; Mo – 26.68; Zr – 4.36 |
| 6 (Co–W–Zr) | 4 | 2/10 | Co – 88.25; W – 9.06; Zr – 2.69 |
| 7 (Co–W–Zr) | 6 | 2/10 | Co – 73.87; W – 24.35; Zr – 1.78 |

the coating.

The analysis of ACM data is indicative of the nano-globular character of the surface of Co–Mo–W coatings on which the cone-shaped associates with the diameter of 2 to 5 μm are formed due to the merging of fine globules with the diameter of 20 to 80 nm. The roughness parameters calculated for the section area of 20×20 μm are: $R_a$ = 0.02, and $R_q$ = 0.04.

Ternary coatings with Co–Mo–Zr alloy differ from Co–Mo–W ones by more branched surface and uniformly distributed cone-shaped associates with the diameter of 5 to 7 μm (fig. 1, *c*, *d*). The cobalt content increases with the current density and an extension of the pulse time. However, the percentage of alloying metals is decreased in comparison with that of Co–Mo–W coatings (table 1, specimens 3–5). Despite this, the origination of cracks in Co–Mo–Zr coatings is independent of the refractory components content as well as of current density. Many studies have paid attention to the cracking of binary and ternary cobalt and molybdenum alloys [30, 31]. A possible cause of the coatings fracturing can be the difference in the crystal lattice types of the alloying metals. It is known that cobalt and zirconium crystal structure is hexagonal close packed (hcp), and molybdenum as well as tungsten are characterized by is body-centered cubic (bcc) crystal lattice. The analysis of the AFM data obtained for Co–Mo–Zr coatings on the section area of 20×20 μm allowed us to calculate the roughness parameters of $R_a$ и $R_q$ that are equal to 0.1 and 0.2, accordingly, and are one order of magnitude higher than those for Co–Mo–W coatings.

The morphology and relief of Co–W–Zr coatings are similar to those of Co–Mo–W coatings (fig. 2, specimens 6, 7); however, the tungsten content reduces in the alloys obtained for the same electrolysis conditions (Table 1, specimens 1 and 2). It should be noted that zirconium percentage in Co–W–Zr is also lower in comparison to that in Co–Mo–Zr coatings deposited under the same conditions (table 1, specimens 3 and 5). A decrease in the size of associates (agglomerates) and unavailability of the cracks in the coatings can be related to the influence of tungsten on the electro-crystallization process. An increase in the current density contributes to the enrichment of the coating with tungsten, though the

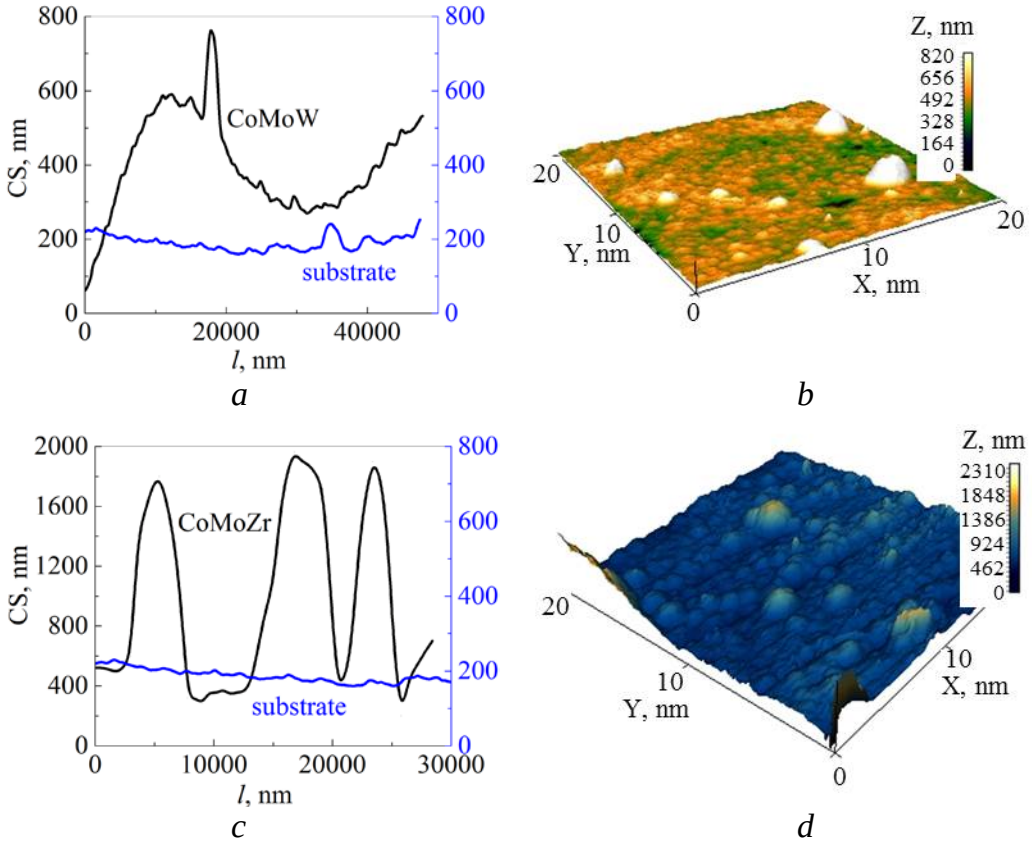


Fig. 1. Topography (*a*, *b*) and the relief (*c*, *d*) of the surface of Co–Mo–W alloy (specimen 1, table 1
(*a*,*b*) and Co–Mo–Zr alloy (specimen 3, table 1 (*c*, *d*).

content of zirconium reduces to 1.78 wt.% (table 1, specimens 6 and 7).

Nevertheless, as shown in [23, 32–34], the relief and a degree of the surface development of all coatings mentioned above are favorable for the catalytic processes that occur not only through the adsorption stage but are also realized in the diffusive mode.

Alongside with the formation of branched globular surface, the phase composition of coatings can turn out to be an important factor that has an effect on their properties, and in particular on the catalytic activity because it predetermines the distribution of active accepting centers on the surface.

Fig.3 gives the X-ray patterns of the ternary coatings Co–Mo–W that are deposited onto the copper substrate in the pulse mode; the coating thickness is 20 μm. The X-ray diffraction patterns reflect the amorphous-and-crystalline alloy structure. The patterns were detected that correspond to the α-Co phase, $Co_7W_6$, $Co_7Mo_6$, and $Co_7Mo_3$ intermetallic compounds. A rather broad halo is visible at the 2θ angles from 43 to 58° (fig. 3) that reflects the X-ray amorphous structure of coatings. The most important event is the origination of the

reflexes of metallic molybdenum and tungsten which are formed in compliance with the mechanism suggested in [8, 9, 22] during the reduction of intermediate oxides by hydrogen ad-atoms when the polarization current is interrupted. The sizes of the zone of coherent dissipation of the amorphous portion of alloy vary in the range of 2 to 8 nm [22].

The X-ray diffraction patterns (fig. 4) show the difference in the phase composition of electrolytic Co–Mo–Zr alloys deposited in the pulse mode of a different current amplitude (see table 1, specimens 3, 5). The figure shows the α-Co lines as well as the lines of intermetallic compounds $Co_3Mo$, $Co_7Mo_3$, $Co_7Mo_6$, and metallic molybdenum (the specimen 3). A narrow halo is observed at the angles of 2θ from 48 to 58° reflecting the amorphous structure of materials. Unavailability of the lines that correspond to zirconium or its intermetallides is explained by the low metal percentage in the coatings. In addition, a high intensity of the lines of intermetallides for the specimen 3 is conditioned by the enrichment of alloy with a refractory component. The sizes of the zone of coherent dissipation of the amorphous portion of alloy vary in the range of 2 to 6 nm [22].

The X-ray diffraction patterns of Co–W–Zr alloys that are deposited in the pulse mode of different current amplitude (specimens 6 and 7, table 1) differ from those for Co–Mo–W and Co–Mo–Zr by unavailability of tungsten and molybdenum metallic phases (fig. 5). The intensity of the lines of $Co_7W_6$ intermetallides increases with the tungsten content. A rather wide halo at the angles of 2θ in the range of 48 to 65° confirms the availability of the X-ray amorphous structure.

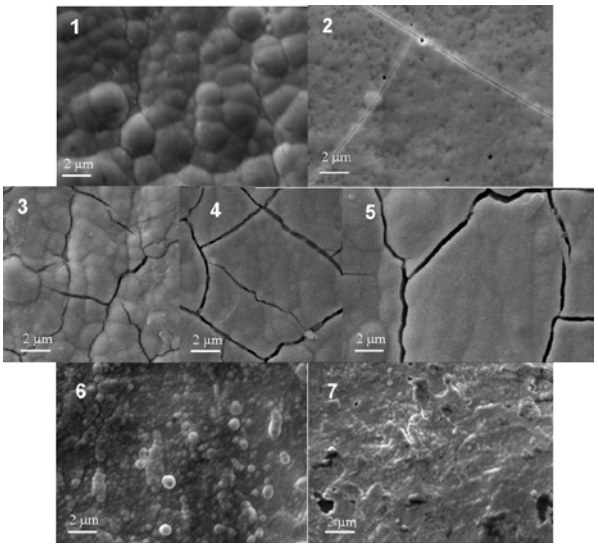


Fig. 2. Morphology of the ternary cobalt coatings surface (SEM photo magnification × 5000). The number of specimens corresponds to that in the table 1.

The size of the zones of coherent dissipation of the amorphous portion of alloy is smaller in comparison to those considered above and equals to 2−5 nm [22].

It is evident that the difference in the surface structure and morphology, as well as in the phase composition of electrolytic alloys, will have an effect on their electrochemical behavior, in particular on the corrosion resistance and catalytic activity in electrode reactions.

The electrochemical impedance spectra (EIS) of the electrodes coated with ternary alloys (fig. 6, 7) in Nyquist coordinates (fig. 6, *a*, 7, *a*) reflect the fact that the systems can be described by the modified Voith equivalent circuit peculiar for multiphase systems [29, 35].

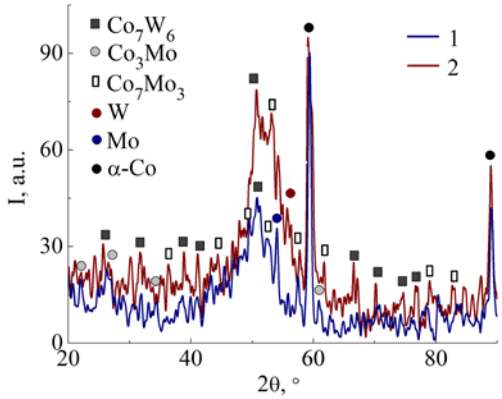


Fig. 3. The X-ray diffraction patterns for ternary Co–Mo–W coatings: 1 is for the specimen 1, and 2 is for the specimen 2 (table 1).

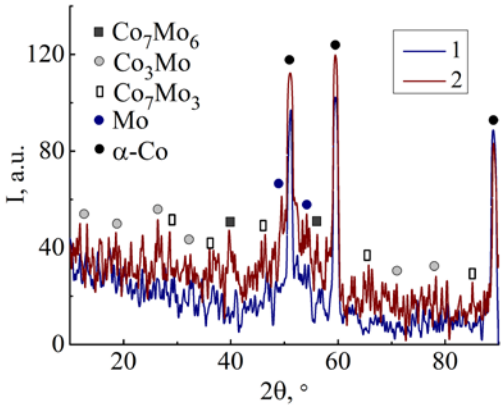


Fig. 4. The X-ray diffraction patterns of ternary Co–Mo–Zr coatings: 1 is for the specimen 5; 2 is for the specimen 3.

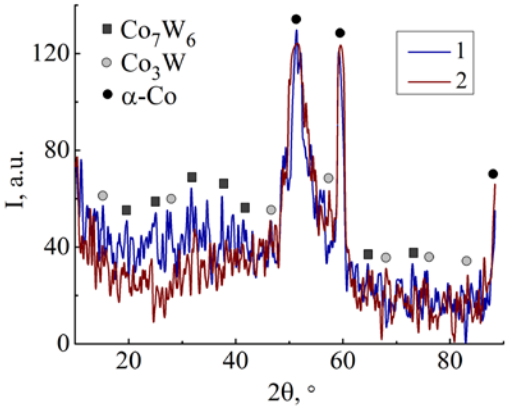


Fig. 5. X-ray diffraction patterns of ternary Co–W–Zr coatings: 1 is for the specimen 7; 2 is for the specimen 6.

The coating corrosion process is associated with formation of oxides of alloying metals on the surface. These nonstoichiometric oxides differ in chemical nature, porosity and electrical conductivity. Therefore, the equivalent circuit includes at least two *R*–*C* chains, one of which corresponds to the oxide phase and the other describes the corrosion behavior of the coating.

Such circuit may include the following elements: *R*1 is associated with the electrolyte resistance; $CPE_i$ ($i$ = 1, 2) is the constant phase element (the phase interface capacity), and $R_i$ ($i$ = 2, 3) is the resistance of oxide layer ($i$ = 2) or corrosion one ($i$ = 3). The CPE elements define the phase fractality that is peculiar for the metals (such as Co, Mo, W) of a variable valence that form hydrated oxide films on the surface in alkali corrosive medium. The degree of deviation from the perfect capacitor (the degree of surface fractality) is determined by the parameter $n$ ($0 < n < 1$), and for the perfect capacitor $n = 1$ [29].

Fig. 6 shows the different shape of Nyquist plots for specimens coated with Co–Mo–W alloy: specimen 1 demonstrates more capacitor behavior in comparison with specimen 2. The equivalent circuit for specimen 1 includes only three elements: the electrolyte resistance *R*1, CPE1 which is associated with oxide layer capacitance, and *R*2 which simulates the resistance of the non-porous oxide layer (fig. 7, *b*). The values of equivalent circuit parameters are: *R*1 = 63±1 Ω cm$^2$; CPE1 = 0.1±0.02 Ω cm$^2$; *R*2 = 9100±1100 Ω cm$^2$.

The Nyquist plot for specimen 2 (fig. 6, *a*) is characterized by two flattened

semi-circles that reflect inhomogeneity of the surface, namely some sections with pores and cracks (see table 1), and as a result of uneven distribution of corrosion process in the system. Therefore, the equivalent circuit for this specimen consists of two *R*–*C* chains (fig. 6, *b*), where the first one reflects the compact oxide layer properties as for the specimen 1. The second chain is associated with corrosion behavior of porous oxide film, where CPE2 is the double layer capacitance, while *R*3 simulates the corrosion resistance, which is inversely proportional to the corrosion rate. The values of equivalent circuit parameters and the error (%) of parameters fitting to the experimental data are given in the table 2. They characterize sample 2 as resistant to corrosion in an alkaline environment, but with decreased ohmic resistance. Both facts are favorable for the implementation of electro-catalytic processes.

The Nyquist plots as well as equivalent circuit for Co–Mo–Zr-coated electrodes (specimens 3–5) are similar to each other and to that of specimen 2, and to Co–W–Zr alloys (fig. 7, *a*). Since the difference of parameters does not exceed the error of 5–7 %, we present data only for specimen 3 (Co–Mo–Zr) and specimen 6 (Co–W–Zr) (table 2) obtained at similar electrolysis conditions. The higher values of *R*2 and *R*3 for specimen 3 in comparison with specimen 2 are due to the presence on the surface of stoichiometric zirconium oxide $ZrO_2$ with high both electrical resistivity and chemical stability.

It should also be noted that the chemical stability of molybdenum oxides in an alkaline medium is higher than that of tungsten. Therefore, the parameters *R*2 and *R*3 for specimen 6 are lower compared to sample 3. The results for Co–Mo–Zr coatings are more reproducible than for Co–Mo–W, which makes possible to consider Co–Mo–Zr alloy as more corrosively stable in an alkaline environment. Moreover, we can conclude that coatings with metallic phases of Mo or W are characterized by higher corrosion resistance.

Obtained EIS data agree with corrosion test results carried out using polarization resistance method in different media for ternary cobalt electrolytic alloys [8–10]. The anodic behavior of ternary coating following from CV in alkaline solution also confirm the high chemical stability of alloys and the ability to quasi-reversible oxidation/ /reduction under external current. Cyclic voltammograms (fig. 8) were obtained by polarizing the electrodes into the cathode region, and then into the anode one. We can see the oxidation peaks in the potential range –(0.7–0.6) on CV for electrodes coated with Co–Mo–W and Co–Mo–Zr (fig. 8, *a* and 8, *b*) after cathodic polarization. These peaks are most likely related to the oxidation of adsorbed at the electrode surface hydrogen atoms formed in the cathodic reaction. Another oxidation peak for those coatings appears in the potential range 0.3–0.4 V, and the anodic current for Co–Mo–W coating is an order of magnitude higher than that of Co–Mo–Zr. Upon reaching a potential of 0.5 V, the passivation of the studied electrodes occurs, and the current density in the passive state doesn't exceed 0.1 $mA/cm^2$ for Co–Mo–Zr, but that for Co–Mo–W is of 2 $mA/cm^2$. The second oxidation peak can be attributed to the formation of alloying

components oxides during anodic polarization. The reverse branch of the CV dependence in fig 8, *b* indicates a quasi-reversible reduction of these oxides, which distinguishes coating Co–Mo–Zr from C–Mo–W (fig. 8, *a*).

The CV for the samples coated with Co–W–Zr alloys differs from those shown

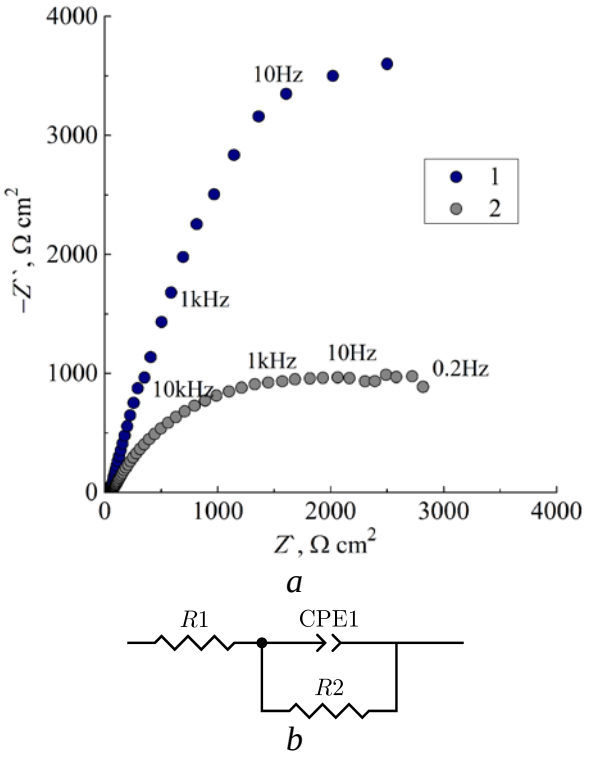


Fig. 6. Nyquist plots (*a*) and the equivalent circuit (*b*) for the Co-Mo-W electrode: 1 is for the specimen 1; 2 is for the specimen 2 (see table 1).

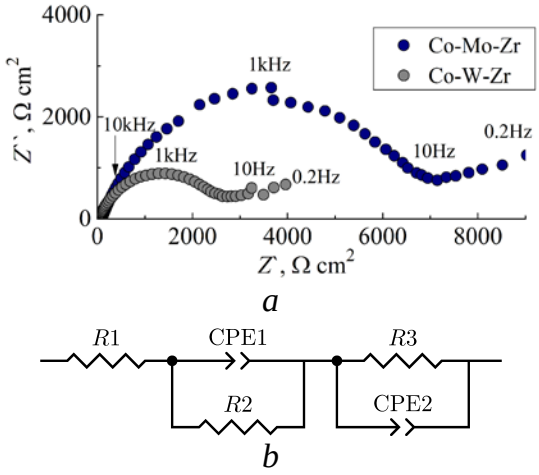


Fig. 7. Nyquist plots (*a*) and the equivalent circuit (*b*) for the Co–Mo–Zr (specimen 3) and Co–W–Zr (specimen 6) electrodes.

above by the appearance of a cathodic peak at potentials of –(0.05–0.3) V, and the current peak reaches 27 mA/cm$^2$. Obviously, the reduction of alloying components oxides unreduced during alloy deposition occurs at cathodic polarization. At the same time, there is no peaks on the anode branch of CV, and the current of the passive state does not exceed 2 mA/cm$^2$ up to the initiation of oxygen evolution at the potential of 0.8 V. We can conclude that the anodic peaks observed for coatings Co–M–W and Co–Mo–Zr are associated with the formation of namely molybdenum oxides, since there is no peak on the anodic branch of CV for Co–W–Zr.

Table 2

**Values of equivalent circuit parameters (Ω cm$^2$) and error (%) of parameters fitting for coated specimens**

| Coating (specimen) | *R*1 | Error | *R*2 | Error | CPE1 | Error | CPE2 | Error | *R*3 | Error | *n* |
|---|---|---|---|---|---|---|---|---|---|---|---|
| Co–Mo–W (2) | 59 | 0.2 | 3700 | 24 | 0.74 | 1.4 | 0.53 | 2.2 | 1800 | 9 | 0.47 |
| Co–Mo–Zr (3) | 61 | 1.2 | 7100 | 1.9 | 0.76 | 0.8 | 0.98 | 2.4 | 2500 | 4 | 0.48 |
| Co–W–Zr (6) | 42 | 0.9 | 2800 | 2.1 | 0.76 | 0.7 | 0.9 | 1.7 | 1300 | 8 | 0.51 |

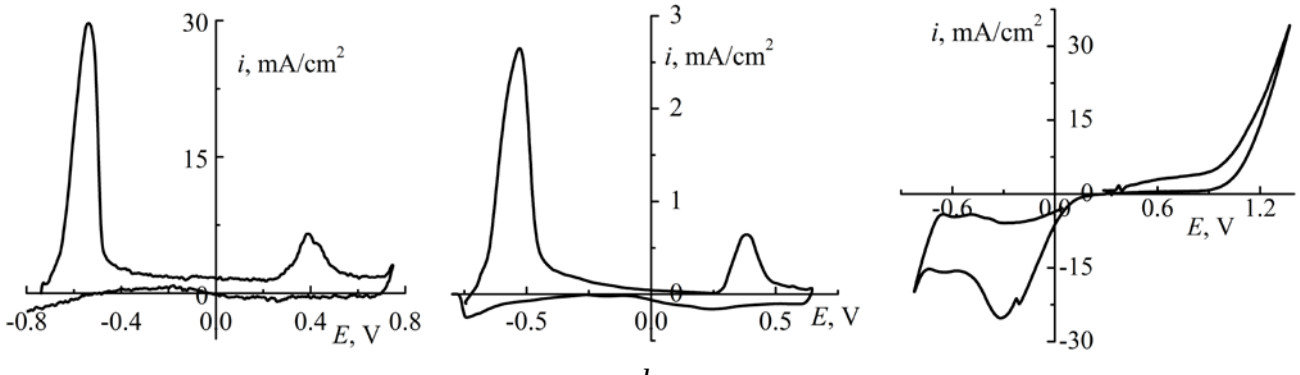


*a* *b* *c*

Fig. 8. Cyclic voltamograms in the 0.25M NaOH solution for electrodes coated with alloys: *a* – Co–Mo–W (specimen 1); *b* – Co–Mo–Zr (specimen 3); *c* – Co–W–Zr (specimen 6).

Observed anodic behavior indicates higher stability of ternary coatings containing zirconium. In addition, it should be noted that an increase in the cobalt content in the alloy (table 1) facilitates its passivation in alkaline environment.

*CONCLUSIONS*. The ternary Co–Mo–W(Zr) coatings with the total content of refractory metals of 30–40 wt.%, and Co–W–Zr alloys with that of 12–26 wt.% are deposited from pyrophosphate-citrate electrolytes in pulse regime. A uniformly cone-shaped surface characterizing the coatings is developed due to tungsten and molybdenum incorporation, but molybdenum containing ternary coatings differs by the network of shallow cracks.

The X-ray diffraction patterns reflect the amorphous-and-crystalline structure of ternary alloys. Phases of α-Co, intermetallic compounds $Co_3Mo$, $Co_7Mo_3$, $Co_7Mo_6$, and traces of metallic molybdenum were detected in the coatings Co–Mo–Zr. Phase composition of Co–Mo–W deposits differs by the emergence of $Co_7W_6$ phase and traces of metallic tungsten, and there is no metallic W in the phase composition of Co–W–Zr electrolytic alloys.

The corrosion behavior of the ternary coatings in alkaline medium studied by EIS shows that the Co–Mo–Zr alloys are characterized by the highest corrosion resistance among the materials studied, and results are more reproducible. Such behavior is due to presence of stoichiometric zirconium oxide $ZrO_2$ on the surface with high both electrical resistivity and chemical stability. We can conclude that coatings Co–Mo–W and Co–Mo–Zr containing metallic phases of Mo or W are characterized by higher corrosion resistance.

Anodic behavior of Co–Mo(W)–Zr coatings in alkali solution is associated with formation of molybdenum oxides during anodic polarization and their quasi-reversible reduction, and indicates higher stability of ternary coatings containing zirconium. Simultaneously, an increase in the cobalt content in the alloy facilitates its passivation in an alkaline medium.

Hence, a high corrosion resistance of Co–Mo–Zr coatings allows us to view them as promising electrode materials for chemical current sources, in particular alkaline fuel cells.

This research was conducted with the support of the Ministry of Education and Science of Ukraine within the confines of the project (Registration Number 0118U002051).

КОРОЗІЙНА ПОВЕДІНКА ЕЛЕКТРОЛІТИЧНИХ ПОТРІЙНИХ СПЛАВІВ КОБАЛЬТУ З Mo(W) ТА Zr У ЛУЖНОМУ РОЗЧИНІ

Т.О.Ненастіна[2], М.В.Ведь[1]*, М.Д.Сахненко[1], І.Ю.Єрмоленко[1], В.О.Проскуріна[1], М.М.Волобуєв[1]

[1]*Національний технічний університет "Харківський політехнічний інститут", вул. Кирпичова, 2, Харків, 61002, Україна*
[2]*Харківський національний автомобільно-дорожній університет, вул.Ярослава Мудрого,25, Харків, 61000, Україна*
**e-mail: vmv@kpi.kharkov.ua*

Потрійні покриття Co–Mo–W (Zr) із загальним вмістом тугоплавких металів 30–40 % мас. та сплави Co–W–Zr (12–26% мас.) осаджено з пірофосфатно-цитратних електролітів у імпульсному режимі. Показано, що склад покриттів, а також морфологія поверхні залежать від густини струму. Рентгенограми відображають структуру потрійних аморфних і кристалічних сплавів. У покриттях Co–Mo–Zr виявлені фази ін.-терметалічних сполук α-Co, Co–Mo та сліди металічного молібдену. Фазовий склад покриттів Co–Mo–W відрізняється виникненням фази $Co_7W_6$ і слідів металевого вольфраму, тоді як в електролітичних сплавах Co–W–Zr металевого W немає. Корозійна поведінка потрійних покриттів у лужному середовищі показує, що сплави Co–Mo–Zr характеризуються найбільшою корозійною стійкістю серед нанесених покриттів завдяки наявності металевого молібдену та стехіометричного $ZrO_2$ з високим електричним опором і хімічною стійкістю. Покриття Co–Mo–W і Co–Mo–Zr, що містять фази Mo або W, характеризуються більшою стійкістю до корозії порівняно з покриттям без металічного молібдену і вольфраму. Дані циклічної вольтамперометрії підтверджують стійкість потрійних покриттів у лужному розчині при анодній поляризації. Такі властивості й розвинена глобулярна поверхня роблять матеріали перспективними для використання як анодів у паливних комірках, зокрема на основі лужних електролітів.

К л ю ч о в і  с л о в а: електроосадження; сплави кобальту; корозійна стійкість; тугоплавкий метал.

КОРРОЗИОННОЕ ПОВЕДЕНИЕ ЭЛЕКТРОЛИТИЧЕСКИХ ТРОЙНЫХ КОБАЛЬТОВЫХ СПЛАВОВ С Mo (W) И Zr В ЩЕЛОЧНОМ РАСТВОРЕ

Т.А.Ненастина[2],М.В.Ведь[1]*,Н.Д.Сахненко[1], И.Ю.Ермоленко[1],В.О.Проскурина[1], М.Н.Волобуев[1]

[1]*Национальный технический университет "Харьковский политехнический институт", ул. Кирпичева, 2, Харьков, 61002, Украина*
[2]*Харьковский национальный автомобильно-дорожный университет, ул. Ярослава Мудрого,25,Харьков, 61000, Украина*
**e-mail: vmv@kpi.kharkov.ua*

Тройные покрытия Co–Mo–W(Zr) с общим содержанием тугоплавких металлов 30–40 % мас. и сплавы Co-W-Zr (12–26 мас.%) получены из пирофосфатно-ци-

тратных электролитов в импульсном режиме. Рентгенограммы отражают структуру аморфно-кристаллических тройных сплавов. В покрытиях Co-Mo-Zr обнаружены фазы α-Co, интерметаллидов Co-Mo и следы металлического молибдена. Фазовый состав Co-Mo-W отличается появлением фазы $Co_7W_6$ и следами металлического W, в сплавах Co-W-Zr отсутствует металлический W. Коррозионное поведение тройных покрытий в щелочной среде свидетельствует о наивысшей коррозионной стойкости сплавов Co-Mo-Zr благодаря присутствию металлического молибдена и стехиометрического $ZrO_2$ с высоким удельным электрическим сопротивлением. Данные циклической вольтамперометрии подтверждают стабильность тройных покрытий в щелочном растворе при анодной поляризации. Такие свойства нанесенных тройных покрытий позволяют рассматривать их как перспективные материалы для использования в качестве анодов в топливных элементах, в частности, на основе щелочных электролитов.

К л ю ч е в ы е  с л о в а: электроосаждение; сплавы кобальта; коррозионная стойкость; тугоплавкий металл.

REFERENCES

1. Averkov I.S., Baykov A.V., Yanovskiy L.S., Volokhov V.M. Modeling of electrochemical processes in solid oxide fuel cells. *Russ. Chem. Bull.* 2017. **65**: 2375.
2. Korovin N.V., Sedlov A.S., Slavnov Y.A., Burov V.D. Calculating the efficiency of a hybrid power station employing a high-temperature fuel cell. *Therm. Eng.* 2007. **54**: 137.
3. Mench M.M. *Fuel Cell Engines.* (New Jersey: John Wiley and Sons Inc., 2008).
4. Liu L., Corma A. Metal Catalysts for Heterogeneous Catalysis: From Single Atoms to Nanoclusters and Nanoparticles. *Chem. Rev*. 2018. **118**: 4981.
5. Greeley J., Nørskov J.K., Mavrikakis M. Electronic Structure and Catalysis On Metal Surfaces. *Annu. Rev. Phys. Chem*. 2002. **53**: 319.
6. Tarasevich M.R., Bogdanovskaya V.A. In: Maiyalagan T, Saji VS (ed) *Electrocatalysts for Low Temperature Fuel Cells: Funda-mentals and Recent Trends.* (KGaA:Wiley-VCH Verlag GmbH & Co, 2017).
7. Ved M., Glushkova M., Sakhnenko N. Catalitic properties of binary and ternary alloys based on silver. *Func. Mater.* 2013. **20**: 87.
8. Sakhnenko N.D., Ved M.V., Hapon Y.K., Nenastina T.A. Functional Coatings of Ternary Alloys of Cobalt with Refractory Metals. *Russ. J. Appl. Chem*. 2015. **88**: 1941.
9. Yar-Mukhamedova G., Ved' M., Sakhnenko N., Nenastina T. Electrodeposition and properties of binary and ternary cobalt alloys with molybdenum and tungsten. *Appl. Surf. Sci.* 2018. **445**: 298.
10. Ved' M.V., Koziar M.A., Sakhnenko N.D., Slavkova M.A. Functional properties of electrolytic alloys of Cobalt with Molybdenum and Zirconium. *Func. Mater*. 2016. **23**(3): 420.
11. Yapontseva Y.S., Dikusar A.I., Kyblanovskii V.S. Study of the composition, corrosion, and catalytic properties of Co-W alloys electrodeposited from a citrate pyrophosphate electrolyte. *Surf. Eng. Appl. Electrochem*. 2014. **50**: 330.

12. Wendlandt A.E., Stahl S.S. Quinone-Catalyzed Selective Oxidation of Organic Molecules. *Angew. Chem. Int. Ed. Engl.* 2015. **54**:14638.

13. Zhang J., Shangguan L., Shuang S., Dong C. Electrocatalytic oxidation of formaldehyde and methanol on $Ni(OH)_2$/Ni electrode. *Russ. J. Electrochem*. 2013. **49**: 888.

14. Song C., Khanfar M., Pickup P. Mo oxide modified catalysts for direct methanol, formaldehyde and formic acid fuel cells. *J. Appl. Electrochem*. 2006. **36**: 339.

15. Pirskyy Y., Murafa N., Korduban O., Šubrt J. Nanostructured catalysts for oxygen electroreduction based on bimetallic monoethanolamine complexes of Co(III) and Ni(II). *J. Appl. Electrochem*. 2014. **44**: 1193.

16. Mejía C.H., van Deelen T.W., de Jong K.P. Activity enhancement of cobalt catalysts by tuning metal-support interactions. *Nature Communications.* 2018. **9**: 4459.

17. Zeng J., Lee J.Y. Effects of preparation conditions on performance of carbon-supported nanosize Pt-Co catalysts for methanol electro-oxidation under acidic conditions. *J. Power Sources*. 2005. **140**: 268.

18. Kharmachi I., Dhouibi L., Berçot P., Rezrazi M. Co-deposition of Ni-Co alloys on carbon steel and corrosion resistance. *J. Mater. Environ. Sci.* 2015. **6**: 1801.

19. Yapontseva Y., Kublanovsky V., Maltseva T. Peculiarities of electrodeposition of Cobalt-Tungsten-Rhenium alloy. *Ukrainian Chemistry Journal*. 2019. **85**: 80.

20. Arzumanova A., Starunov A., Shpanova K. Wear Resistance of a Composite Galvanic Coating Based on the Nickel-Cobalt Alloy. *Materials Science Forum*. 2019. **945**: 735.

21. Garcia J., Lago D., Senna L. Electrodeposition of Cobalt Rich Zn-Co alloy Coatings from Citrate Bath. *Materials Research*. 2014. **17**: 947.

22. Ved' M.V., Sakhnenko N.D., Yermolenko I.Y., Nenastina T.A. *Nanostructured Functional Coatings of Iron Family Metals with Refractory Elements*. In: Fesenko O., Yatsenko L. (ed.) Nanochemistry, Biotechnology, Nanomaterials, and Their Applications. (Cham: Springer, 2018).

23. Ved' M.V., Sakhnenko M.D., Bohoyavlens'ka O.V., Nenastina T.O. Modeling of the surface treatment of passive metals. *Mater. Sci*. 2008. **44**: 79.

24. Yar-Mukhamedova G., Sakhnenko N., Ved' M., Yermolenko I., Zyubanova S. Surface analysis of Fe-Co-Mo electrolytic coatings. *IOP Conference Series: Materials Science and Engineering*, 2017. **213**.

25. Ved' M.V., Sakhnenko M.D., Karakurkchi H.V., Ermolenko I.Yu., Fomina L.P. Functional Properties of Fe-Mo and Fe-Mo-W Galvanic Alloys. *Mater. Sci*. 2016. **51**: 701.

26. Yermolenko I.Y., Ved' M.V., Sakhnenko N.D., Sachanova Y.I. Composition, Morphology, and Topography of Galvanic Coatings Fe-Co-W and Fe-Co-Mo. *Nanoscale Res. Lett*. 2017. **12**:352.

27. Thomas D., Rasheed Z., Jagan J.S., Kumar K.G. Study of kinetic parameters and development of a voltammetric sensor for the determination of butylated

hydroxyanisole (BHA) in oil samples. *J. Food Sci. Technol.* 2015. **52**:6719.

28. Dutta G., Siddiqui Sh., Zeng H., Carlisle J., Arumugam P. The effect of electrode size and surface heterogeneity on electrochemical properties of ultrana-nocrystalline diamond microelectrode. *J. Electroanal. Chem*. 2015. **756**: 61.
29. Cesiulis H., Tsyntsaru N., Ramanavicius A., Ragoisha G. In: Tiginyanu I. (ed.), NanoScience and Technology. (Springer Nature, Switzerland AG, 2016).
30. Casciano P.N.S., Ramon L. Benevides R.L., Santana R.A.C. Factorial design in the electrodeposition of Co-Mo coatings and their evaluations for hydrogen evolution reaction. *J. Alloys Compd*. 2016. **723**: 164.
31. Kublanovsky V.S., Yapontseva Y.S. Electro-catalytic Properties of Co-Mo Alloys Electrodeposited from a Citrate-Pyro-phosphate Electrolyte. *Electrocatal.* 2014. **5**: 372.
32. Ved M., Sakhnenko N., Bairachnaya T., Tkachenko N. Structure and properties of electrolytic cobalt-tungsten alloy coatings. *Func. Mater*. 2008. **15**: 613.
33. Yermolenko I.Y., Ved' M.V., Sakhnenko N.D., Fomina L.P., Shipkova I.G. Galvanic ternary Fe-Co-W coatings: structure, composition and magnetic properties. *Func. Mater*. 2018. **25**: 274-281.
34. Yakushin R., Kuterbekov K., Grafov D., Kuterbekov K., Nurakhmetov T., Yakushin R. Improving the Efficiency and Safety of Operation of the Hydrogen Fuel Cell. *Safety in Technosphere*. 2015. **3**: 40.
35. Chiu H.W., Chuang J.M., Lu C.C., Lin W.T., Lin C.W., Lin M.L. In situ measurement of tissue impedance using an inductive coupling interface circuit. *IEEE Trans. Biomed. Circuits Syst*. 2013. **7**: 225.

Received 25.10.2019